Distributed Laser Charging: A Wireless Power Transfer Approach

Qingqing Zhang, *Student Member, IEEE*, Wen Fang, Qingwen Liu, *Senior Member, IEEE*, Jun Wu, *Senior Member, IEEE*, Pengfei Xia, *Senior Member, IEEE*, and Liuqing Yang, *Fellow, IEEE*

***Abstract*—Wireless power transfer (WPT) is a promising solution to provide convenient and perpetual energy supplies to electronics. Traditional WPT technologies face the challenge of providing Watt-level power over meter-level distance for Internet of Things (IoT) and mobile devices, such as sensors, controllers, smart-phones, laptops, etc. Distributed laser charging (DLC), a new WPT alternative, has the potential to solve these problems and enable WPT with the similar experience as WiFi communications. In this paper, we present a multimodule DLC system model, in order to illustrate its physical fundamentals and mathematical formula. This analytical modeling enables the evaluation of power conversion or transmission for each individual module, considering the impacts of laser wavelength, transmission attenuation, and photovoltaic-cell (PV-cell) temperature. Based on the linear approximation of electricity-to-laser and laser-to-electricity power conversion validated by measurement and simulation, we derive the maximum power transmission efficiency in closed-form. Thus, we demonstrate the variation of the maximum power transmission efficiency depending on the supply power at the transmitter, laser wavelength, transmission distance, and PV-cell temperature. Similar to the maximization of information transmission capacity in wireless information transfer (WIT), the maximization of the power transmission efficiency is equally important in WPT. Therefore, this paper not only provides the insight of DLC in theory, but also offers the guideline of DLC system design in practice.**

***Index Terms*—Distributed laser charging (DLC), power transmission efficiency, wireless power transfer (WPT).**

I. Introduction

INTERNET of Things (IoT) and mobile devices, such as sensors and smart-phones, are typically powered by batteries that have limited operation time. Sensors for IoT, especially sensors that being deployed in special environments such as volcanoes, are difficult to be charged. Meanwhile, carrying a power cord and looking for a power supplier to charge mobile devices incur great inconvenience. An alternative is thus to transfer power wirelessly, which virtually provides perpetual energy supplies. Hence, wireless power transfer (WPT) or wireless charging attracts great attention recently.

Three major wireless charging technologies are surveyed in [1] and [2]. Inductive coupling is safe and simple for implementation. However, it is limited by a short charging distance from a few millimeters to centimeters, which is only suitable for contact-charging devices like toothbrush. Magnetic resonance coupling has high charging efficiency. However, it is restricted by short charging distances and big coil sizes, which fits home appliances like TV. Electromagnetic (EM) radiation has long effective charging distances. However, it suffers from low charging efficiency and is unsafe when the EM power density exposure is high, hence is only favorable for low-power devices like sensors. In a nutshell, these traditional WPT technologies provide great wireless charging abilities for different application scenarios, whereas it is still challenging to offer sufficient power over long distance for safely charging IoT and mobile devices, e.g., smart-sensor, smart-phone, laptop, drone, etc., which usually need Watt-level power over meter-level distances.

To support the power and distance requirements for IoT and mobile devices, a distributed laser charging (DLC) system is presented in [3], which could transfer 2-W power over a 5-m distance [4]. By using inductive coupling or magnetic resonance coupling, IoT, and mobile devices, say sensors and smart-phones, should typically be placed in a special charging cradle with a particular position. However, the DLC's self-aligning feature provides a more convenient way of charging IoT and mobile devices without specific positioning or tracking, as long as the transmitter and the receiver are in the line of sight (LOS) of each other. Different from EM radiation, DLC's WPT can be stopped immediately when this LOS is blocked by any object, which ensures the safety of DLC system. The size of the DLC receiver is sufficiently small to be embedded in a sensor or a smart-phone. The DLC transmitter can be installed on the ceiling like a lightbulb. In addition, multiple devices can be charged simultaneously by a single DLC transmitter [5]–[7]. Therefore, DLC can provide IoT and mobile devices with safe WPT capability, which enables people to charge their devices with the similar experience as WiFi communications.

Fig. 1 illustrates the DLC potential applications. In Fig. 1, in the room, DLC transmitter-1 is combined with a light-emitting diode array and become a DLC-equipped lightbulb. Thus transmitter-1 can be conveniently installed on the ceiling, and

Manuscript received August 10, 2017; revised May 7, 2018; accepted June 19, 2018. Date of publication June 27, 2018; date of current version November 14, 2018. *(Corresponding author: Qingwen Liu.)*

Q. Zhang, W. Fang, Q. Liu, J. Wu, and P. Xia are with the College of Electronic and Information Engineering, Tongji University, Shanghai 201804, China (e-mail: anne@tongji.edu.cn; wen.fang@tongji.edu.cn; qingwen.liu@gmail.com; wujun@tongji.edu.cn; pengfei.xia@gmail.com).

L. Yang is with the Department of Electrical and Computer Engineering, Colorado State University, Fort Collins, CO 80523 USA (e-mail: lqyang@engr.colostate.edu).

Digital Object Identifier 10.1109/JIOT.2018.2851070

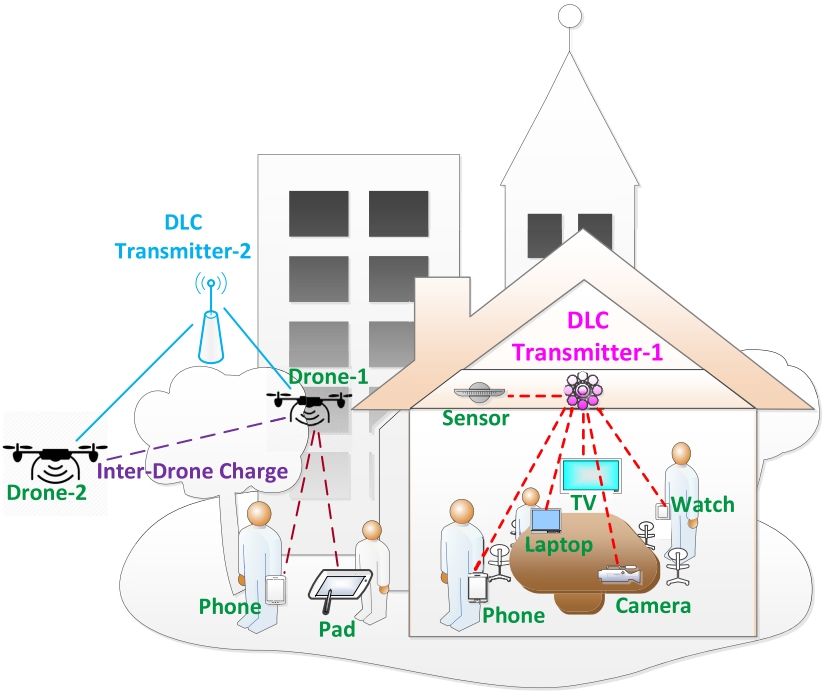

Fig. 1. DLC applications.

then provide wireless power to IoT and mobile devices within its coverage. In the outdoor scenario, drone-1 is equipped with a DLC transmitter, which can charge IoT and mobile devices on demand. At the same time, a DLC receiver is also embedded in drone-1. Thus, it can be remotely charged by DLC transmitter-2, which acts as the power-supply base station on the ground. In addition, drone-2 equipped with both DLC transmitter and receiver can play the role of a relay to receive power from DLC transmitter-2 and transmit power to drone-1 simultaneously.

Similar to the maximization of the *information transmission capacity* of wireless channels in wireless information transfer, an important research topic in WPT is to maximize the *power or energy transmission efficiency* [8]. The wireless charging efficiency of a DLC system is affected by many factors, including laser wavelength, electricity-to-laser conversion efficiency, laser transmission attenuation, and laser-to-electricity conversion efficiency [9]–[12]. In this paper, we focus our study on the modeling of DLC system and its performance evaluation. In order to understand the fundamental mechanism of DLC system, we separate the DLC system into multiple conceptually independent modules. Thus, the corresponding power conversion or transmission for each module can be investigated individually, considering the impacts of laser wavelength, transmission attenuation, and photovoltaic-cell (PV-cell) temperature. Finally, the maximum power transmission efficiency in closed-form can be obtained from this modular analysis.

In this paper, a multimodule system model is proposed to describe the DLC system. The physical mechanism and mathematical formula are presented to describe the relationship between the stimulating electrical power and the output power, as well as the efficiency. The relationship between the supply power and the laser power, the relationship between the received laser power and the output power, and thus the relationship between the output power and the supply power are all depicted by both analytical results and illustrative graphs. The relationship between the electricity-to-laser conversion efficiency and the supply power, the relationship between the laser-to-electricity conversion efficiency and the received laser power, and thus the relationship between the maximum power transmission efficiency and the supply power are captured by closed-form expressions as well as being illustrated by figures. As a result, this paper not only provides the insight of DLC in theory, but also offers the design guideline for DLC system implementation in practice.

In the rest of this paper, we will first review the DLC system and present the multimodule system model. Then, we will illustrate the analytical modeling of each module to investigate the corresponding working principles. After that, we will evaluate the performance of each module and derive the maximum DLC power transmission efficiency in closed-form. Finally, we will give summarizing remarks and discuss open issues for future research.

II. DLC System

DLC is a WPT technology based on the distributed resonating laser presented in [3]. Traditional laser systems belong to the scope of *integrated resonating laser*, since all optical components are integrated in one single device. However, in DLC systems, the optical components are divided into two separate parts, the transmitter and the receiver, respectively. Therefore, the laser in DLC systems falls within the scope of *distributed resonating laser*.

Fig. 2 shows the DLC system diagram described in [3]. A retro-reflector mirror R1 with 100% reflectivity and a gain

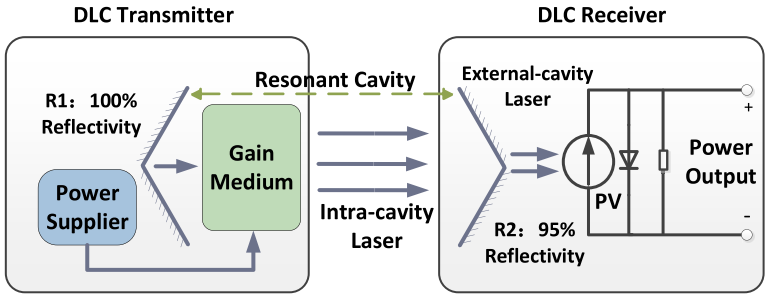

Fig. 2. DLC system diagram.

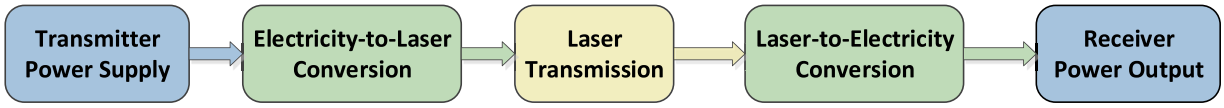

Fig. 3. DLC system model.

medium are implemented at the transmitter. While in the receiver, a retro-reflector mirror R2 with exemplary 95% partial reflectivity is contained. R1, R2, and the gain medium consist the resonant cavity, within which photons are amplified and form intracavity resonating laser. Photons that pass through R2 generates the external-cavity laser. The external-cavity laser power can be converted to electrical power by a photovoltaic-panel (PV-panel) installed behind mirror R2, which is similar to a solar panel. Fig. 2 includes the power supplier at the transmitter and the power output at the receiver for the comprehensive DLC system design.

As specified in [3], in the DLC system, photons is amplified without concerning about the incident angle, as long as they travel along LOS of R1 and R2. Hence, the intracavity laser generated by the resonator can be self-aligned without specific positioning or tracking. This feature enables users to charge their devices without placing them in a specific position cautiously. Besides self-alignment, the DLC system is intrinsically safe, since objects blocking the LOS of intracavity laser can stop the laser immediately. These features offer DLC the capability of safely charging devices over long distance.

Fig. 3 presents the system model to elaborate the WPT in the DLC system. This model illustrates a theoretical framework of power transfer by electricity-to-laser conversion, laser transmission, and laser-to-electricity conversion. The physical fundamentals and mathematical formulations of this modular model will be specified in the following section.

III. Analytical Modeling

In this section, we will discuss each module of the DLC model in Fig. 3 and describe its WPT mechanism analytically. At the DLC transmitter, the power supplier provides electrical power to generate the intracavity laser. We will first introduce the electricity-to-laser conversion. Then, the intracavity laser will travel through the air and arrive at the DLC receiver. We will discuss the intracavity laser power attenuation along its transmission. At the DLC receiver, the intracavity laser will partially go through the mirror R2 and form the external-cavity laser, then the external-cavity laser will be converted into electricity by a PV-panel. We will analyze this laser-to-electricity conversion based on the PV engineering. Finally, the PV-panel output electrical power can be used to charge electronics. Based on the above analytical modeling, we will obtain the power conversion and transmission efficiency of each module and the overall power transmission efficiency.

A. Electricity-to-Laser Conversion

At the DLC transmitter, the electrical power P_s is provided by the power supplier, which depends on the stimulating current I_t and voltage V_t as

$$P_s = I_t V_t. \tag{1}$$

The supply power P_s can stimulate the gain medium to generate laser. Thus, the electrical power can be converted to the laser power. We denote P_l as the external-cavity laser power when the intracavity laser transmission efficiency is 100%. It is well-known that laser can be generated, only when I_t provided by the power supplier is over a certain threshold [13]. In the laser diode physics, the laser power P_l relies on I_t. Their relationship can be depicted as [13]

$$P_l = \zeta \frac{h\upsilon}{q}(I_t - I_{\text{th}}) \tag{2}$$

where ζ is the modified coefficient, h is the Plunk constant, υ is the laser frequency, q is the electronic charge constant, and I_{th} is the current threshold.

Thus, the electricity-to-laser conversion efficiency η_{el} can be figured out as

$$\eta_{\text{el}} = \frac{P_l}{P_s}. \tag{3}$$

B. Laser Transmission

Laser power transmission attenuation means that laser power decreases along with its transmission through the air, which is similar to EM wave propagation power loss [14]. The laser power attenuation level depends on the transmission distance and air quality [15], [16]. Relying on the above laser-generation mechanism, the intracavity laser can transmit

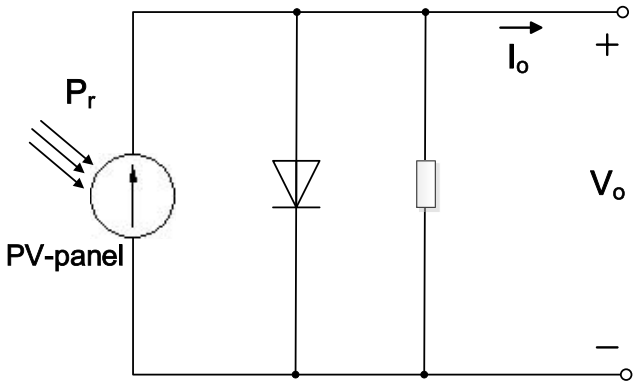

Fig. 4. PV-panel power conversion circuit model.

from the transmitter to the receiver. During the transmission, laser may experience power attenuation. For simplicity, we assume that the laser diameter is a constant. This assumption could be validated by controlling aperture diameters of the DLC transmitter and receiver [15].

The laser transmission efficiency $\eta_{\rm lt}$ can be modeled as [15]

$$\eta_{\rm lt} = \frac{P_r}{P_l} = e^{-\alpha d} \tag{4}$$

where P_r is the external-cavity laser power received at the DLC receiver, α is the laser attenuation coefficient, and d is the distance. When d is close to zero, the laser transmission efficiency approaches 100%. In this situation, P_r is approximate to P_l.

α can be depicted as

$$\alpha = \frac{\sigma}{\kappa}\left(\frac{\lambda}{\chi}\right)^{-\rho} \tag{5}$$

where σ and χ are two constants, κ is the visibility, λ is the wavelength, and ρ is the size distribution of the scattering particles. ρ depends on visibility, which will be discussed later.

C. Laser-to-Electricity Conversion

At the DLC receiver, the external-cavity laser power can be converted to electrical power. To illustrate the laser-to-electricity conversion mechanism, the single-diode equivalent circuit model of a PV-panel is depicted in Fig. 4 [17]. The PV-panel output voltage V_o, and current I_o can be characterized as [17]

$$I_o = I_{\rm sc} - I_s\left(e^{V_o/V_m} - 1\right) \tag{6}$$

where $I_{\rm sc}$ is the PV-panel short-circuit current, I_s is the saturation current, i.e., the diode leakage current density in the absence of light, and V_m is the "thermal voltage," which can be defined as

$$V_m = \frac{nkT}{q} \tag{7}$$

where n is the PV-panel ideality factor, k is the Boltzmann constant, and T is the absolute PV-cell temperature. Then, the PV-panel output power P_o, which relies on I_o and V_o, can be obtained as

$$P_o = I_o V_o. \tag{8}$$

TABLE I
TRANSMISSION OR CONVERSION EFFICIENCY

Parameter	Symbol
Electricity-to-laser conversion efficiency	η_{el}
Laser transmission efficiency	η_{lt}
Laser-to-electricity conversion efficiency	η_{le}
The overall DLC power transmission efficiency	η_o

Therefore, the laser-to-electricity conversion efficiency, i.e., the PV-panel conversion efficiency, $\eta_{\rm le}$ depends on P_o and P_r, which can be depicted as

$$\eta_{\rm le} = \frac{P_o}{P_r} = \frac{I_o V_o}{P_r}. \tag{9}$$

In summary, the PV-panel converts the received laser power P_r to the output power P_o with the efficiency $\eta_{\rm le}$.

D. DLC Power Transmission Efficiency

Based on the above analysis for each individual module of the DLC system model, the DLC power transmission efficiency from the power supplier at the transmitter to the power output at the receiver can be depicted as

$$\eta_o = \eta_{\rm el}\eta_{\rm lt}\eta_{\rm le}. \tag{10}$$

The conversion or transmission efficiency of each module and the DLC power transmission efficiency are listed in Table I.

The numerical evaluation of the DLC system model will be presented in Section IV.

IV. NUMERICAL EVALUATION

Based on the analytical modeling in the previous section, we can find that the DLC system efficiency varies with laser wavelength, transmission attenuation, and PV-cell temperature. Their impacts on the performance of each module as well as the overall DLC system will be discussed in this section. The numerical evaluation is implemented in MATLAB and Simulink.

A. Electricity-to-Laser Conversion

Electrical supply power P_s provided by the power supplier at the transmitter depending on the stimulating current I_t and voltage V_t, as in (1). Based on the measurement of I_t, V_t, and thus P_s, for the laser systems (λ is 800–820 and 1540–1560 nm, respectively) in [9] and [10], the measured supply power P_s, the measured laser power P_l, the stimulating current I_t, and the stimulating voltage V_t are shown for 810 and 1550 nm in Figs. 5 and 6, respectively. From the dashed-lines for the measured laser power in Figs. 5 and 6, the modified coefficient ζ in (2) can be determined and listed in Table II. Thus, from (2), the formulated laser power curves are given as the solid-lines in Figs. 5 and 6, respectively.

In Figs. 5 and 6, the relationship between P_l and P_s is illustrated in Fig. 7. We adopt the linear formula to approximate this power conversion as

$$P_l \approx a_1 P_s + b_1. \tag{11}$$

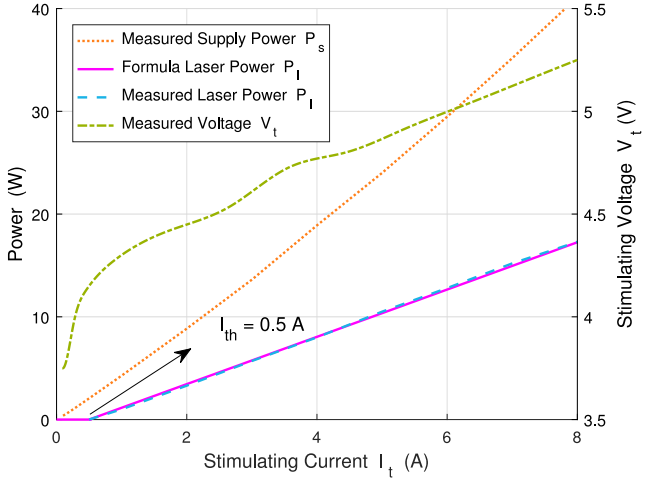

Fig. 5. Electricity-to-laser conversion power, voltage, and current (810 nm).

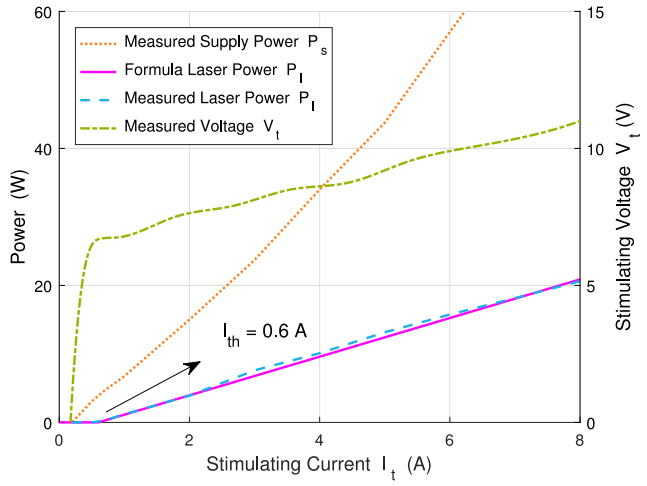

Fig. 6. Electricity-to-laser conversion power, voltage, and current (1550 nm).

TABLE II
ELECTRICITY-TO-LASER CONVERSION PARAMETERS

Parameter	Symbol	Value	
		810nm	1550nm
Boltzmann constant	k	$1.38064852 \times 10^{-23} J/K$	
Planck constant	h	$6.62606957 \times 10^{-34} J \cdot s$	
Electronic charge constant	q	$1.6 \times 10^{-19} C$	
Laser wavelength	λ	$810nm$	$1550nm$
Laser frequency	υ	$3.7 \times 10^{14} Hz$	$1.9 \times 10^{14} Hz$
Stimulation current threshold	I_{th}	$0.5A$	$0.6A$
Modified coefficient	ζ	1.5	3.52
P_l-P_s curve fitting parameter	a_1	0.445	0.34
P_l-P_s curve fitting parameter	b_1	-0.75	-1.1

The measured and formulated curves in Fig. 7 depict the linear approximation between P_l and P_s based on (11), when the wavelength λ is about 810 and 1550 nm, respectively. We can find that the fitting curves match the measurement very well in the given supply power and laser power range in Fig. 7.

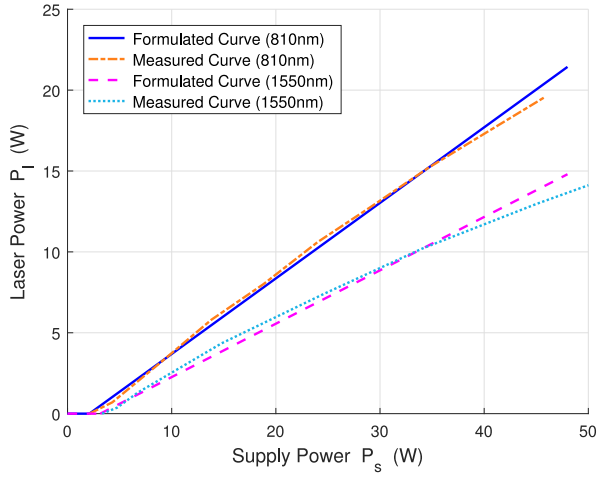

Fig. 7. Laser power versus supply power.

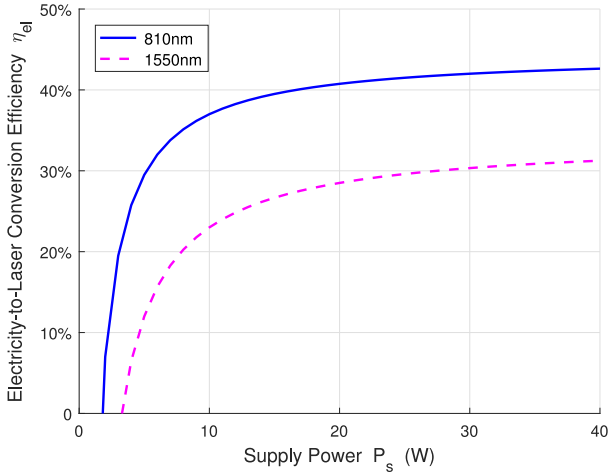

Fig. 8. Electricity-to-laser conversion efficiency versus supply power.

TABLE III
LASER TRANSMISSION PARAMETERS

Parameter	Value		
	Clear Air	Haze	Fog
σ		3.92	
χ		$550nm$	
κ	$10km$	$3km$	$0.4km$
ρ	1.3	$0.16\kappa + 0.34$	0

From (3) and (11), we can obtain the electricity-to-laser conversion efficiency η_{el} as

$$\eta_{\text{el}} = \frac{P_l}{P_s} = a_1 + \frac{b_1}{P_s}. \tag{12}$$

The solid-line and dashed-line in Fig. 8 illustrate η_{el} for 810 and 1550 nm, respectively. The initial P_s supply power threshold in Fig. 8 is corresponding to the current threshold I_{th} for P_l in Figs. 5 and 6. In Fig. 8, η_{el} starts to increase dramatically from the initial supply power P_s threshold and will reach the plateau as P_s increases. The plateau of η_{el} for 810-nm laser is around 43%, which is higher than 31% for 1550-nm laser.

TABLE IV
LASER-TO-ELECTRICITY CONVERSION PARAMETERS

Parameter	Symbol	Value	
		810nm	1550nm
Short-circuit current	I_{sc}	$0.16732A$	$0.305A$
Open-circuit voltage	V_{oc}	$1.2V$	$0.464V$
Irradiance used for measurement	I_{r0}	$36.5W/cm^2$	$2.7187W/cm^2$
Laser frequency	υ	$3.7037 \times 10^{14}Hz$	$1.9355 \times 10^{14}Hz$
Quality factor	n	1.5	1.1
Number of series cells	N	72	
PV-panel material		GaAs-based	GaSb-based
Measurement temperature	T	$25°C$	$120°C$
Simulation temperature		$0°C$ / $25°C$ / $50°C$	
P_m-P_r curve fitting parameter	a_2	0.5455 / 0.5414 / 0.5372	0.5434 / 0.4979 / 0.4525
P_m-P_r curve fitting parameter	b_2	-0.2129 / -0.2313 / -0.2493	-0.2761 / -0.2989 / -0.3209

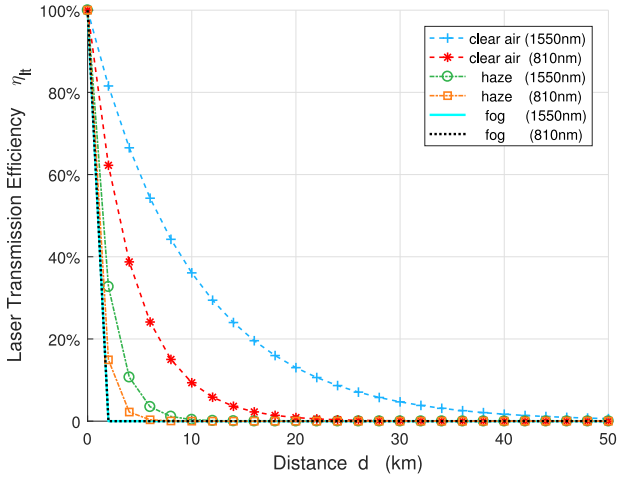

Fig. 9. Laser transmission efficiency versus distance.

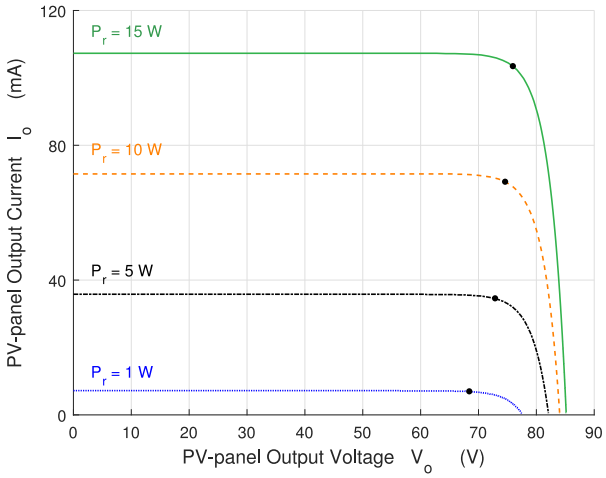

Fig. 10. PV-panel output current versus voltage ($\lambda = 810$ nm).

B. Laser Transmission

From (4) and (5), the laser power attenuation coefficient in transmission can be determined under three typical scenarios, i.e., clear air, haze, and fog. For the three scenarios, the size distribution of the scattering particles ρ in (5) can be specified as [16]

$$\rho = \begin{cases} 1.3, & \text{for clear air} \quad (6 \text{ km} \le \kappa \le 50 \text{ km}) \\ 0.16\kappa + 0.34, & \text{for haze} \quad (1 \text{ km} \le \kappa \le 6 \text{ km}) \\ 0, & \text{for fog} \quad (\kappa \le 0.5 \text{ km}) \end{cases} \tag{13}$$

where κ is the visibility.

Along with ρ, the other attenuation parameters are listed in Table III. Thus, the relationship between η_{lt} and the transmission distance d can be obtained from (4) and (5), which is illustrated in Fig. 9. It is clear that η_{lt} decays exponentially to zero as d increases. Meanwhile, for the same laser wavelength, laser power attenuation depends on the visibility κ. Laser power attenuation increases when κ decreases. As can be seen in Fig. 9, for clear air, haze, and fog, given the same d, the laser power attenuation for short-wavelength is more than that of long-wavelength. For clear air and haze, laser attenuation for 810 nm is much more than that of 1550 nm. However, for fog, since ρ takes 0 for both 810 and 1550 nm, the coefficient α has the same value. Therefore, the laser attenuation in fog does not dependent on λ.

C. Laser-to-Electricity Conversion

At the DLC receiver, PV-panel takes the role of converting laser power to electrical power. PV-panel conversion efficiency relies on laser power, wavelength, and cell temperature. With reference to (6) and (7), we can obtain the PV-panel output current, voltage, and thus power, given the parameters listed in Table IV. Figs. 10–17 demonstrate their relationships for different laser wavelength using the standard *solar cell* Simulink model [18].

Fig. 10 shows the relationship between PV-panel output current I_o and voltage V_o with different input laser power, i.e., the external-cavity laser power P_r at the receiver, for the GaAs-based PV-panel with 810-nm laser at 25 °C [19]. Similarly, Fig. 11 is for the GaSb-based PV-panel with 1550-nm laser at 25 °C [20]. The PV-panel output power P_o can be derived from the corresponding I_o and V_o based on Figs. 10 and 11. Thus, Figs. 12 and 13 depict the relationship between P_o and V_o for 810 and 1550 nm, respectively.

From Figs. 12 and 13, given P_r, we can figure out the maximum output power, which is defined as the maximum power point (MPP) and marked by the dots on the corresponding output power curves. We denote P_m as the MPP

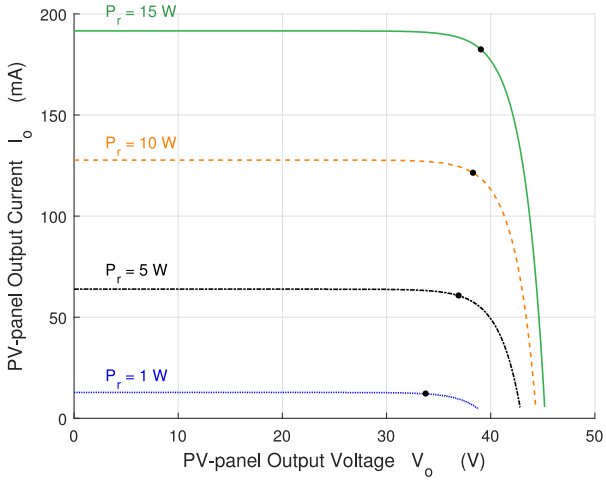

Fig. 11. PV-panel output current versus voltage ($\lambda = 1550$ nm).

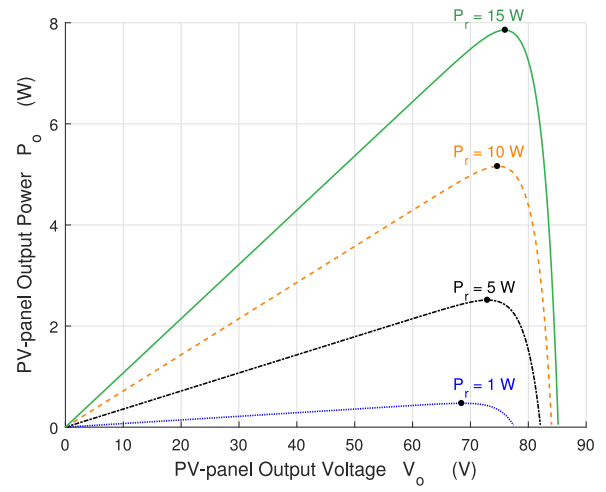

Fig. 12. PV-panel output power versus voltage ($\lambda = 810$ nm).

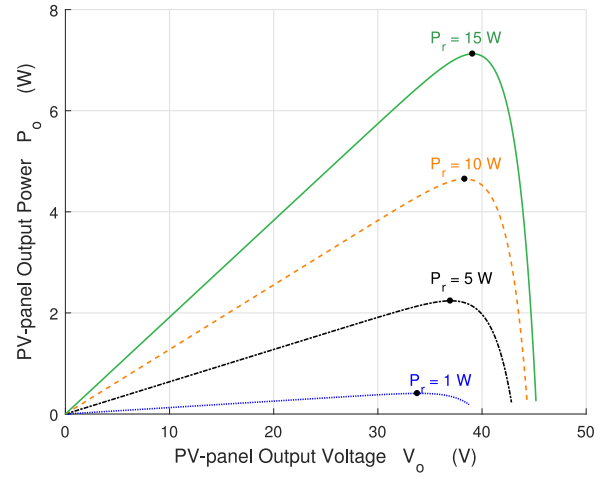

Fig. 13. PV-panel output power versus voltage ($\lambda = 1550$ nm).

of P_o. From [21], P_m is proved as the unique output power, i.e., the corresponding current and voltage are unique, given the received laser power P_r. For example, given $P_r = 10$ W, the MPP is unique as 4.64 W for 1550 nm, which is depicted

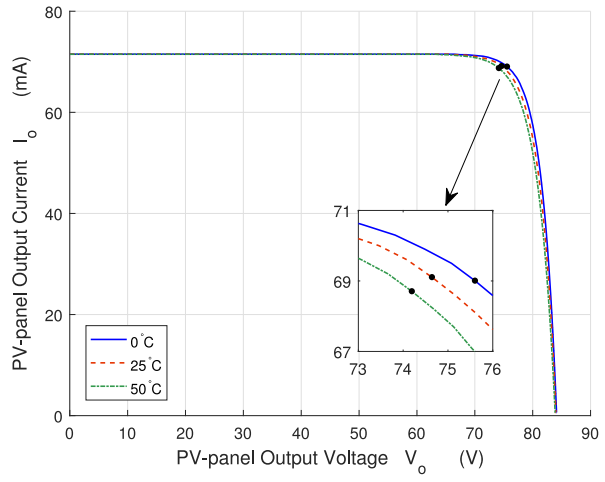

Fig. 14. PV-panel output current versus voltage ($\lambda = 810$ nm).

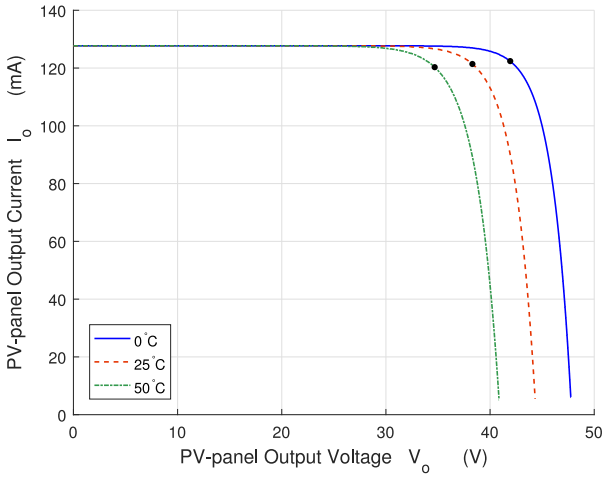

Fig. 15. PV-panel output current versus voltage ($\lambda = 1550$ nm).

by the dots in Figs. 11 and 13. The corresponding unique I_o and V_o are 121.3 mA and 38.3 V, respectively.

In Figs. 10 and 11, given P_r, I_o keeps almost a constant when V_o is below the MPP. However, I_o drops rapidly when V_o is over the MPP. For the same V_o, I_o increases when P_r increases. When I_o is close to zero, V_o is the open-circuit voltage, which increases when P_r increases. From Figs. 12 and 13, given P_r, P_o increases when V_o increases until it reaches the MPP. However, P_o drops dramatically when V_o is above the corresponding voltage for MPP. For a given voltage V_o, the output power P_o increases when the input laser power P_r increases.

Besides input laser power, PV-cell temperature also impacts the PV-panel output current, voltage, and power. Given the three cell temperatures (0 °C, 25 °C, and 50 °C), for $\lambda = 810$ nm and $P_r = 10$ W power, Figs. 14 and 16 depict the variation of I_o and P_o on different V_o, respectively. Similarly, for $\lambda = 1550$ nm and $P_r = 10$ W power, Figs. 15 and 17 show the PV-panel output I_o, V_o, and P_o for these cell temperatures.

From Figs. 14 and 15, I_o keeps almost as a constant when V_o is below a certain value. Given different cell temperatures, I_o curves start dropping at different V_o. The turning voltage is low when the temperature is high. From Figs. 16 and 17, P_o

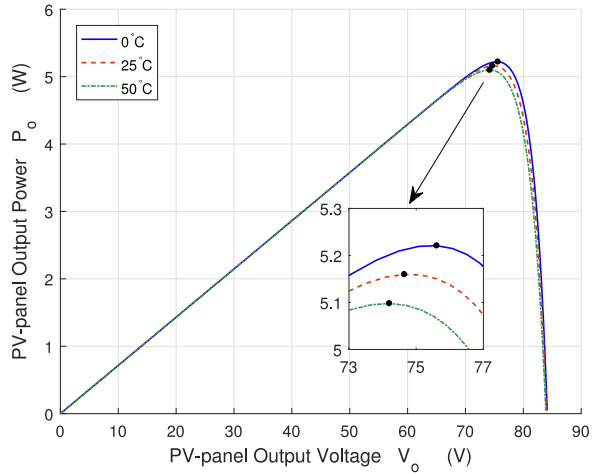

Fig. 16. PV-panel output power versus voltage ($\lambda = 810$ nm).

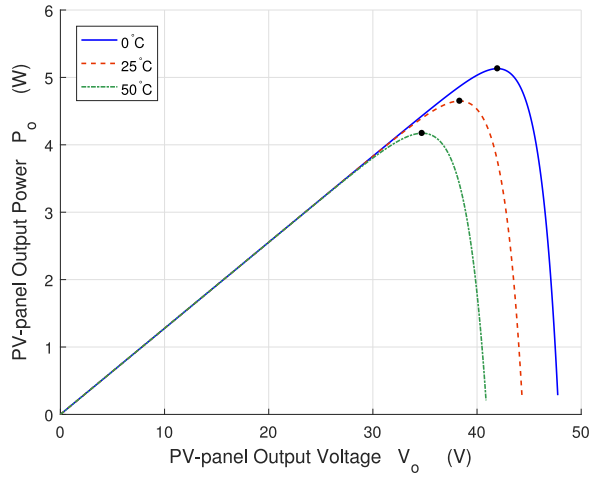

Fig. 17. PV-panel output power versus voltage ($\lambda = 1550$ nm).

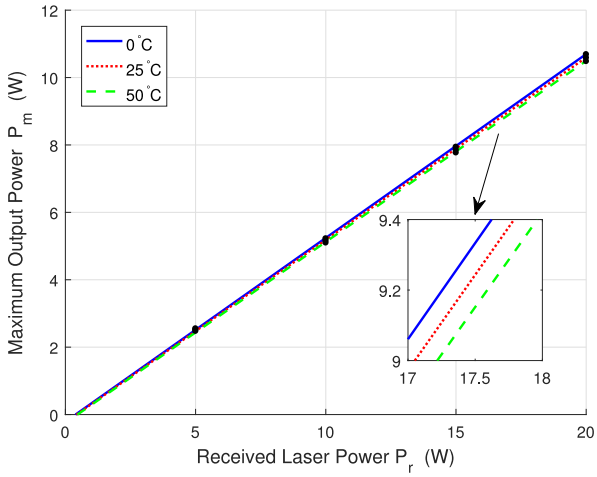

Fig. 18. Maximum output power versus received laser power ($\lambda = 810$ nm).

is low when the temperature is high. Additionally, the MPP increases as the cell temperature declines.

Based on the MPP dots in Figs. 10 and 12 for different P_r and Figs. 14 and 16 for different cell temperatures, we can obtain the MPP dots in Fig. 18, which illustrates P_m versus

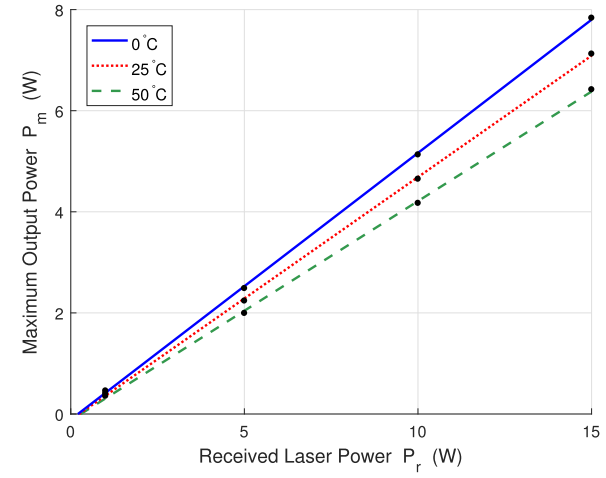

Fig. 19. Maximum output power versus received laser power ($\lambda = 1550$ nm).

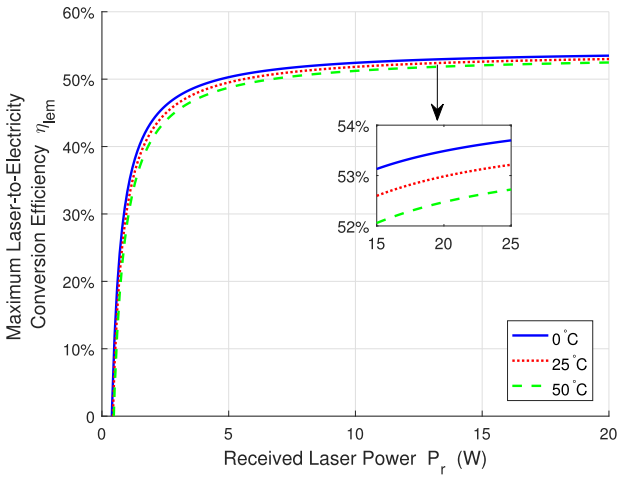

Fig. 20. Maximum laser-to-electricity conversion efficiency versus received laser power ($\lambda = 810$ nm).

P_r for 810 nm. Similarly, Fig. 19 demonstrates P_m versus P_r for 1550 nm. In order to evaluate the relationship between P_m and P_r, we adopt the approximation formula by using the curve fitting method as

$$P_m \approx a_2 P_r + b_2 \tag{14}$$

where a_2 and b_2 are the linear curve fitting coefficients for different wavelengths and cell temperatures, which are listed in Table IV. From Figs. 18 and 19, we can find that the approximate lines based on (14) matches the MPP dots very well.

We denote η_{lem} as the maximum PV-panel conversion efficiency when P_o is P_m. Based on (9) and (14), η_{lem} can be depicted as

$$\eta_{lem} = \frac{P_m}{P_r} = a_2 + \frac{b_2}{P_r}. \tag{15}$$

Figs. 20 and 21 show how η_{lem} varies with the received laser power P_r for 810 and 1550 nm, respectively. From Figs. 20 and 21, the changing trend of η_{lem} is similar with that of η_{el} in Fig. 8. η_{lem} is low when cell temperature is high. The

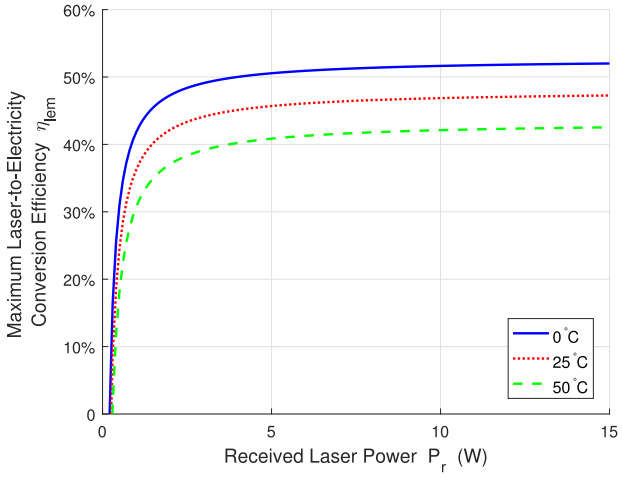

Fig. 21. Maximum laser-to-electricity conversion efficiency versus received laser power ($\lambda = 1550$ nm).

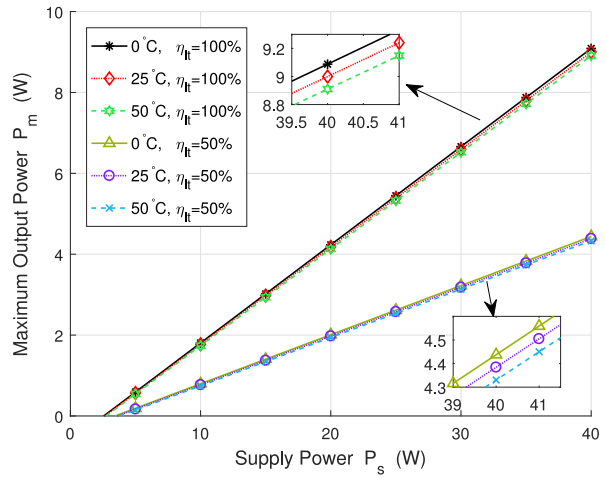

Fig. 22. Maximum output power versus supply power ($\lambda = 810$ nm).

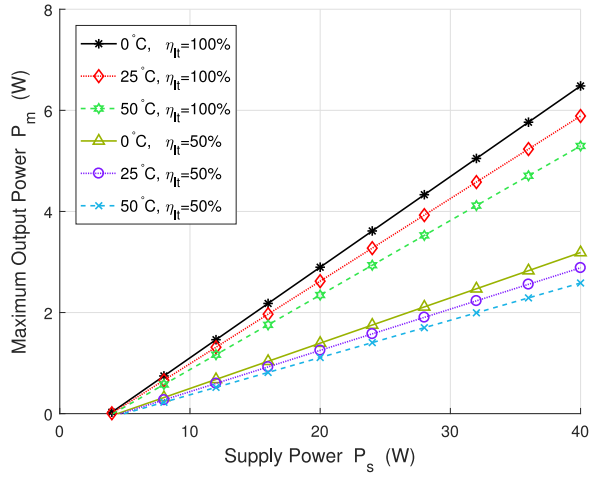

Fig. 23. Maximum output power versus supply power ($\lambda = 1550$ nm).

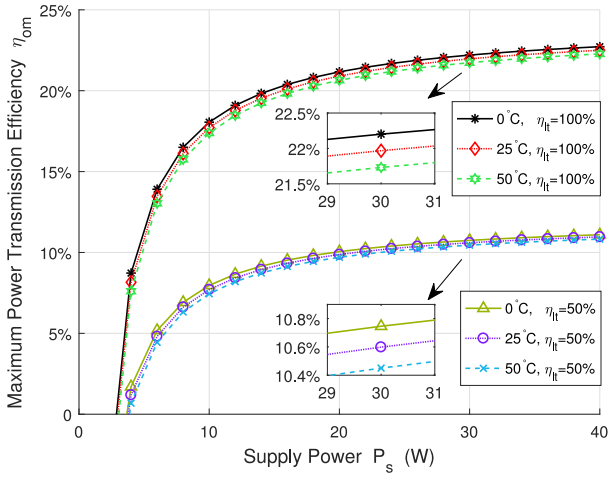

Fig. 24. Maximum power transmission efficiency versus supply power ($\lambda = 810$ nm).

impact of cell temperature on η_{lem} is bigger for 1550 nm than that of 810 nm, comparing Figs. 20 and 21.

D. DLC Power Transmission Efficiency

The relationship between the laser power P_l and the supply power P_s is demonstrated by (11), when the transmission distance d is close to zero in the electricity-to-laser conversion. The relationship between P_l and the received laser power P_r due to laser transmission is illustrated in (4). The relationship between P_r and the maximum PV-panel output power P_m in the laser-to-electricity conversion is shown in (14). Thus, from (4), (11), and (14), we can obtain the relationship between P_s at the transmitter and P_m at the receiver as

$$P_m = a_2\eta_{\rm lt}P_l + b_2 = a_1a_2\eta_{\rm lt}P_s + (a_2b_1\eta_{\rm lt} + b_2). \quad (16)$$

Fig. 22 depicts the linear relationship between P_m and P_s for $\eta_{\rm lt} = 100\%$ and $\eta_{\rm lt} = 50\%$, respectively, when PV-cell temperature is 0 °C, 25 °C, 50 °C, and $\lambda = 810$ nm. Meanwhile, Fig. 23 illustrates the similar circumstances for $\lambda = 1550$ nm.

From (10), we denote η_{om} as the maximum power transmission efficiency, when P_o is P_m, i.e., $\eta_{\rm le}$ approaches η_{lem}. From (3), (4), (9), (10), (12), and (15), the maximum power transmission efficiency η_{lem} can be obtained as

$$\begin{aligned}\eta_{om} &= \eta_{\rm el}\eta_{\rm lt}\eta_{lem} \\ &= \eta_{\rm el}\eta_{\rm lt}\left(a_2 + \frac{b_2}{\eta_{\rm el}\eta_{\rm lt}P_s}\right) \\ &= a_1a_2\eta_{\rm lt} + \frac{a_2b_1\eta_{\rm lt} + b_2}{P_s} \\ &= a_1a_2e^{-\alpha d} + \frac{a_2b_1e^{-\alpha d} + b_2}{P_s}. \end{aligned} \quad (17)$$

Fig. 24 shows the relationship between η_{om} and P_s when $\eta_{\rm lt}$ are 100% and 50% and cell temperatures are 0 °C, 25 °C, and 50 °C for 810 nm. Fig. 25 shows the same circumstances for 1550 nm. η_{om} raises up with P_s increasing at first, then it reaches the plateau. The growth pattern of η_{om} in Figs. 24 and 25 is similar as $\eta_{\rm el}$ in Fig. 8 and η_{lem} in Figs. 20 and 21.

η_{om} depends not only on the supply power P_s but also on the distance d. Fig. 26 depicts the relationship between η_{om} and d for different laser wavelength and PV-cell temperature,

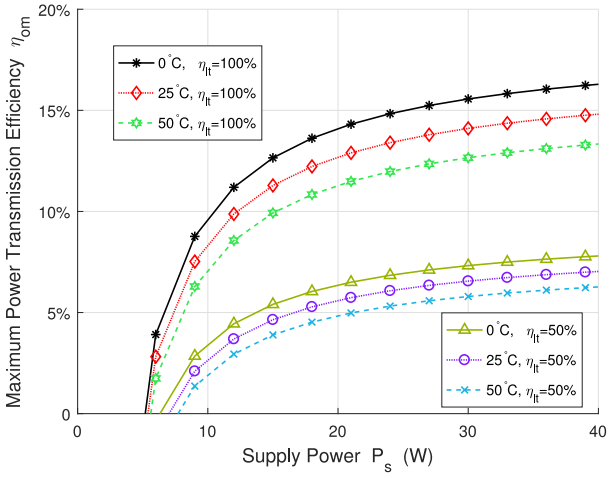

Fig. 25. Maximum power transmission efficiency versus supply power (λ = 1550 nm).

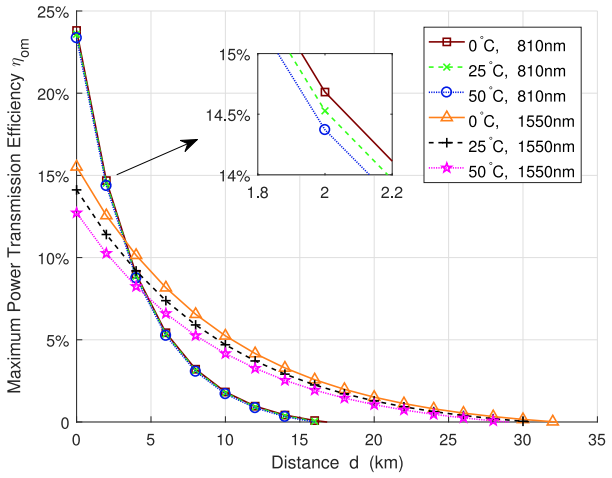

Fig. 26. Maximum power transmission efficiency versus distance (clear air).

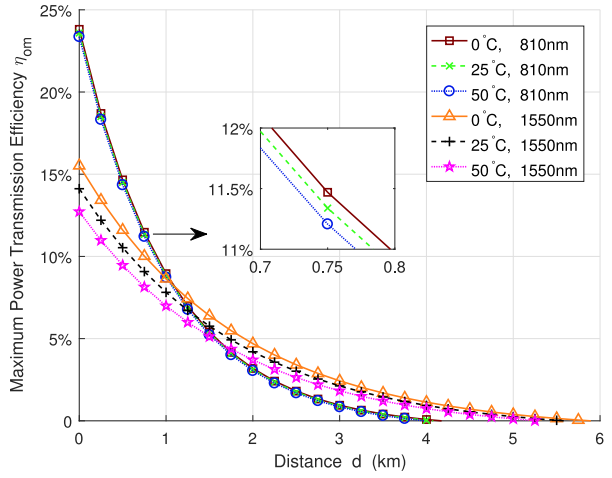

Fig. 27. Maximum power transmission efficiency versus distance (haze).

when P_s = 40 W and air quality is clear. Figs. 27 and 28 illustrate η_{om} for the similar situation when air condition is haze and fog, respectively. Fig. 29 describes how η_{om} changes over η_{lt} under clear air when P_s is 40 W.

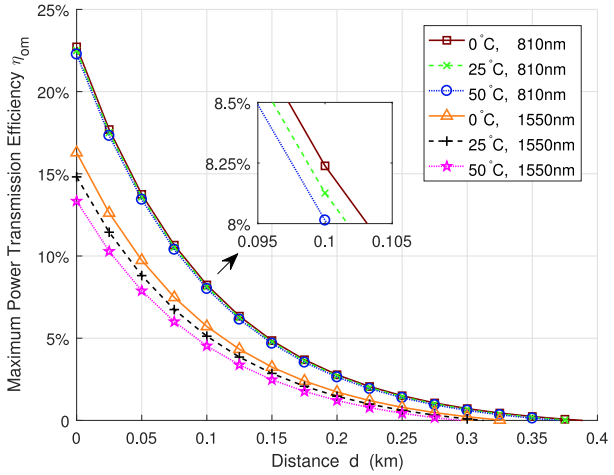

Fig. 28. Maximum power transmission efficiency versus distance (fog).

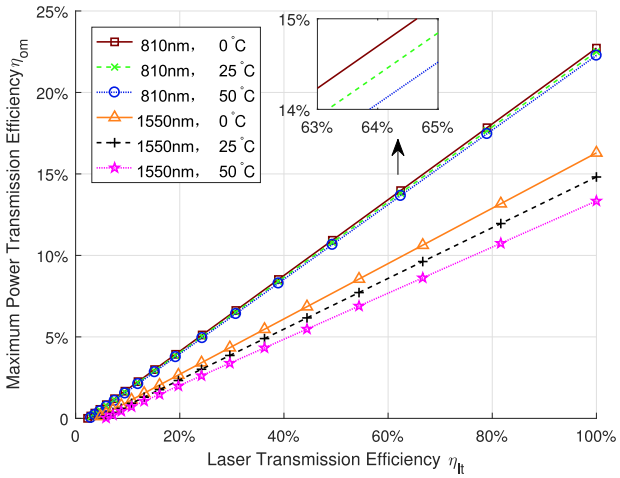

Fig. 29. Maximum power transmission efficiency versus laser transmission efficiency.

From Figs. 26 and 27, η_{om} decreases when d increases. η_{om} of 810-nm laser is higher than that of 1550-nm laser when d is short. However, η_{om} for 810 nm is lower than that of 1550 nm when d is long. From Fig. 28, η_{om} of 810-nm laser always keep higher than that of 1550-nm laser until η_{om} decrease to 0. At the same time, as described above, the cell temperature has bigger impact on η_{om} for 1550 nm than that of 810 nm.

From Fig. 29, η_{om} increases linearly as η_{lt} enhances based on (17). Fig. 29 provides a guideline of designing the DLC systems. For example, if 20% of DLC maximum transmission efficiency is expected, the 1550-nm DLC system cannot meet the requirement; however, the 810-nm DLC system is preferred. Meanwhile, when deploying the DLC system, the transmission efficiency at a certain distance provides the theoretical reference to determine the radius, i.e., the coverage, which is similar to the base station coverage analysis in mobile communications [22], [23]. Therefore, the maximum economic benefits can be obtained by minimizing the number of DLC transmitters to cover a given area [24]. This analysis provides a guideline for the efficient deployment of the DLC systems.

In summary, the numerical evaluation in this section validates the analytical model presented in Section III. At first,

for the three modules: electricity-to-laser conversion, laser transmission, laser-to-electricity conversion, the conversion or transmission efficiency of each module is quantitatively analyzed. Second, through numerical analysis, we obtain the approximate linear relationship between the supply power P_s at the transmitter and the maximum PV-panel output power P_m at the receiver. Next, the maximum DLC power transmission efficiency η_{om} in closed-form is derived. Finally, based on the maximum power transmission efficiency, DLC system design and development guidelines are provided, for example, how to select the laser wavelength and determine the coverage of the DLC systems.

V. Conclusion

This paper presents the DLC technology for WPT. The multimodule analytical modeling of DLC provides the in-depth view of its physical mechanism and mathematical formulation. The numerical evaluation illustrates the power conversion or transmission in each module under the impacts of laser wavelength, transmission attenuation, and PV-cell temperature. The linear approximation is adopted and validated by measurement and simulation for electricity-to-laser and laser-to-electricity power conversion. Thus the maximum power transmission efficiency in closed-form is derived and its performance depending on the supply power, laser wavelength, transmission distance, and PV-cell temperature is illustrated by figures. Therefore, this paper not only provides the theoretical insight, but also offers the practical guideline in system design and deployment of DLC.

Due to the space limitation, there are serval important issues unaddressed in this paper and left for our future work, some of which are briefly discussed here.

1) The PV-panel efficiency used in the DLC system is about 50%, which is not much efficient. More studies on the PV-panel types, the efficiency analyzation, and the total efficiency of the DLC system could be improved in the future.
2) Only 810- and 1550-nm laser wavelengths are considered in this paper. Wider range of wavelengths can be studied to make the DLC system more universal in the future work.
3) To convert the PV-panel output current and voltage to different preferred charging current and voltage for different applications, the circuit or device that can convert a source of direct current from one voltage level to another is worth to be discussed in the future.
4) The point-to-point charging procedure is well illustrated in this paper. On this basis, the accessing protocols, the scheduling algorithms, the influencing factors of power conversion and transmission, and the system optimization for charging batteries adaptively in the point-to-multiple-point wireless charging scenario should be another interesting topic to discuss.
5) Since point-to-multiple-point WPT is naturally supported by DLC systems, the network architecture of WPT becomes an interesting research topic worthy of further investigation. The related protocols and algorithms to effectively operate WPT networks could be developed, e.g., WPT network access protocols, WPT scheduling algorithms, and so on [1].
6) It is interesting to investigate the potential simultaneous wireless information and power transfer (SWIPT) in DLC systems. Due to the huge available bandwidth conveyed by laser, such high-power and high-rate SWIPT systems have the potential to support the demanding applications, e.g., IoT, mobile virtual reality/augmented reality, ultrahigh-definition video streaming, and so on [8].

References

[1] X. Lu, D. Niyato, P. Wang, D. I. Kim, and Z. Han, "Wireless charger networking for mobile devices: Fundamentals, standards, and applications," *IEEE Wireless Commun.*, vol. 22, no. 2, pp. 126–135, Apr. 2015.

[2] A. Costanzo *et al.*, "Electromagnetic energy harvesting and wireless power transmission: A unified approach," *Proc. IEEE*, vol. 102, no. 11, pp. 1692–1711, Nov. 2014.

[3] Q. Liu *et al.*, "Charging unplugged: Will distributed laser charging for mobile wireless power transfer work?" *IEEE Veh. Technol. Mag.*, vol. 11, no. 4, pp. 36–45, Dec. 2016.

[4] Western Coalfields Limited Technology. (Jun. 2017). *To Power With Light*. [Online]. Available: http://www.wi-charge.com/

[5] J. Gong, S. Zhou, and Z. Niu, "Optimal power allocation for energy harvesting and power grid coexisting wireless communication systems," *IEEE Trans. Commun.*, vol. 61, no. 7, pp. 3040–3049, Jul. 2013.

[6] A. Scaglione and Y.-W. Hong, "Opportunistic large arrays: Cooperative transmission in wireless multihop ad hoc networks to reach far distances," *IEEE Trans. Signal Process.*, vol. 51, no. 8, pp. 2082–2092, Aug. 2003.

[7] S. Zhou, Z. Wang, and G. B. Giannakis, "Performance analysis for transmit-beamforming with finite-rate feedback," in *Proc. 38th Conf. Info. Sci. Syst.*, 2004, pp. 17–19.

[8] R. Zhang and C. K. Ho, "MIMO broadcasting for simultaneous wireless information and power transfer," *IEEE Trans. Wireless Commun.*, vol. 12, no. 5, pp. 1989–2001, May 2013.

[9] LDSCM Technologies. (Jul. 2017). *Laser Diode Source—808nm*. [Online]. Available: https://www.laserdiodesource.com/shop/808nm-25Watt-Laser-Diode-Module-BWT-Beijing

[10] Laser Diode Source Seminex. (Jul. 2017). *Laser Diode Source—1550nm*. [Online]. Available: https://www.laserdiodesource.com/laser-diode-product-page/1470nm-1532nm-1550nm-50W-multi-chip-fiber-coupled-module-Seminex

[11] L. Summerer and O. Purcell, *Concepts for Wireless Energy Transmission Via Laser*, Eur. Space Agency (ESA), Adv. Concepts Team, Noordwijk, The Netherlands, 2009.

[12] A. G. Martin, E. Keith, H. Yoshihiro, W. Wilhelm, and D. D. Ewan, "Solar cell efficiency tables (version 45)," *Progr. Photovoltaics Res. Appl.*, vol. 23, no. 1, pp. 1–9, 2015.

[13] B. V. Zeghbroeck, *Principles of Semiconductor Devices*, 1st ed. Boulder, CO, USA: Univ. Colorado, 2004.

[14] S. A. Salman, J. M. Khalel, and W. H. Abas, "Attenuation of infrared laser beam propagation in the atmosphere," *Diala J.*, vol. 36, pp. 2–9, 2009.

[15] J. M. Liu, *Semiconductor Lasers and Light Emitting Diodes*, 1st ed. New York, NY, USA: Univ. Rochester, 2005.

[16] I. I. Kim, B. McArthur, and E. J. Korevaar, "Comparison of laser beam propagation at 785 nm and 1550 nm in fog and haze for optical wireless communications," in *Proc. SPIE*, vol. 4214. Boston, MA, USA, 2001, pp. 26–37.

[17] M. S. Aziz, S. Ahmad, I. Husnain, A. Hassan, and U. Saleem, "Simulation and experimental investigation of the characteristics of a PV-harvester under different conditions," in *Proc. IEEE Int. Conf. Energy Syst. Policies (ICESP)*, Nov. 2014, pp. 1–8.

[18] T. Salmi, M. Bouzguenda, A. Gastli, and A. Masmoudi, "MATLAB/Simulink based modeling of photovoltaic cell," *Int. J. Renew. Energy Res. (IJRER)*, vol. 2, no. 2, pp. 213–218, 2012.

[19] E. Oliv, F. Dimroth, and A. W. Bett, "GaAs converters for high power densities of laser illumination," *Progr. Photovoltaics Res. Appl.*, vol. 16, no. 4, pp. 289–295, 2008.
[20] V. P. Khvostikov, S. V. Sorokina, F. Y. Soldatenkov, and N. K. Timoshina, "GaSb-based photovoltaic laser-power converter for the wavelength $\lambda \approx 1550$ nm," *Semiconductors*, vol. 49, no. 8, pp. 1079–1082, Aug. 2015.
[21] S. Liu and R. A. Dougal, "Dynamic multiphysics model for solar array," *IEEE Trans. Energy Convers.*, vol. 17, no. 2, pp. 285–294, Jun. 2002.
[22] Z. Zhou, S. Zhou, J.-H. Cui, and S. Cui, "Energy-efficient cooperative communication based on power control and selective single-relay in wireless sensor networks," *IEEE Trans. Wireless Commun.*, vol. 7, no. 8, pp. 3066–3078, Aug. 2008.
[23] K.-L. Noh, Q. M. Chaudhari, E. Serpedin, and B. W. Suter, "Novel clock phase offset and skew estimation using two-way timing message exchanges for wireless sensor networks," *IEEE Trans. Commun.*, vol. 55, no. 4, pp. 766–777, Apr. 2007.
[24] Q. Liu, W. Zhang, X. Ma, and G. T. Zhou, "A practical amplify-and-forward relaying strategywith an intentional peak power limit," in *Proc. Int. Conf. Acoust. Speech Signal Process.*, 2010, pp. 2518–2521.

Qingqing Zhang (S'16) received the M.E. degree in computer science and technology from the Hunan University of Technology, Hunan, China, in 2016. She is currently pursuing the Ph.D. degree at the College of Electronics and Information Engineering, Tongji University, Shanghai, China.

Her current research interests include wireless charge, wireless power transfer, simultaneous wireless information and power transmission, Internet of Things, and communications.

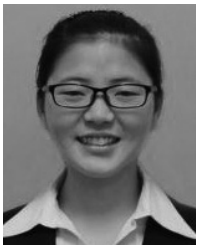

Wen Fang received the B.S. degree in computer science and technology from the Shandong University of Science and Technology, Qingdao, China, in 2017. She is currently pursuing the Ph.D. degree at the College of Electronics and Information Engineering, Tongji University, Shanghai, China.

Her current research interests include wireless power transmission, development of remote wireless charging technology, Internet of Things, and financial transactions.

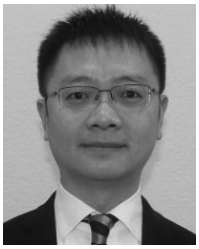

Qingwen Liu (M'07–SM'15) received the B.S. degree in electrical engineering and information science from the University of Science and Technology of China, Hefei, China, in 2001, and the M.S. and Ph.D. degrees from the Department of Electrical and Computer Engineering, University of Minnesota, Minneapolis, MN, USA, in 2003 and 2006, respectively.

He is currently a Professor with the College of Electronics and Information Engineering, Tongji University, Shanghai, China. His current research interests include wireless power transfer and Internet of Things.

Jun Wu (M'03–SM'14) received the B.S. degree in information engineering and M.S. degree in communication and electronic systems from Xidian University, Xi'an, China, in 1993 and 1996, respectively, and the Ph.D. degree in signal and information processing from the Beijing University of Posts and Telecommunications, Beijing, China, in 1999.

He was a Principal Scientist with Huawei, Shenzhen, China, and Broadcom, Irvine, CA, USA. He joined the College of Electronics and Information Engineering, Tongji University, Shanghai, China, as a Professor in 2010. His current research interests include wireless communication, information theory, and multimedia signal processing.

Pengfei Xia (S'03–M'05–SM'10) received the Ph.D. degree from the Department of Electrical and Computer Engineering, University of Minnesota, Minneapolis, MN, USA, in 2005.

He is currently a Full Chair Professor with the College of Electronics and Information, Tongji University, Shanghai, China. He co-edited *60 GHz Technology for Gb/s WLAN and WPAN: From Theory to Practice* (Wiley, 2011). His current research interests include wireless communications, networks, and signal processing.

Dr. Xia was a co-recipient of the IEEE Signal Processing Society Best Paper Award in 2011. He currently serves as a Signal Processing for Communications (SPCOM) Technical Committee member and the SPCOM Industrial/Government Subcommittee Chair for the IEEE Signal Processing Society.

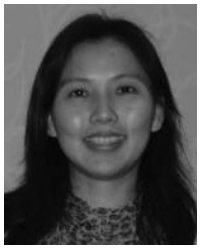

Liuqing Yang (S'02–M'04–SM'06–F'15) received the Ph.D. degree in electronics and computer engineering from the University of Minnesota, Minneapolis, MN, USA, in 2004.

She is currently a Professor with Colorado State University, Fort Collins, CO, USA. Her current research interests include signal processing in communications, network, and energy systems.

Dr. Yang was a recipient of the IEEE ICUWB'06, ICCC'13, ITSC'14, Globecom'14, ICC'16, and WCSP'16 Best Paper Award. She also serves as an Associate Editor/Senior Editor for various journals, such as the IEEE TRANSACTIONS ON COMMUNICATIONS, the IEEE TRANSACTIONS ON WIRELESS COMMUNICATIONS, the IEEE TRANSACTIONS ON SIGNAL PROCESSING, the IEEE TRANSACTIONS ON INTELLIGENT TRANSPORT SYSTEM, *IEEE Intelligent Systems*, and an Associate Editor of *PHYCOM: Physical Communication*. She is a Distinguished Lecturer for ITSS and ComSoc.